

# MAGNETOHYDRODYNAMIC SIMULATIONS OF RECONNECTION AND PARTICLE ACCELERATION: THREE-DIMENSIONAL EFFECTS

GRZEGORZ KOWAL<sup>1,3</sup>, E. M. DE GOUVEIA DAL PINO<sup>1</sup> & A. LAZARIAN<sup>2</sup>

<sup>1</sup>Instituto de Astronomia, Geofísica e Ciências Atmosféricas, Universidade de São Paulo, Rua do Matão 1226, 05508-900, São Paulo, Brazil

<sup>2</sup>Department of Astronomy, University of Wisconsin, 475 North Charter Street, Madison, WI 53706, USA and

<sup>3</sup>Obserwatorium Astronomiczne, Uniwersytet Jagielloński, ul. Orla 171, 30-244 Kraków, Poland

*Draft version April 3, 2024*

## ABSTRACT

The magnetic fields can change their topology through a process known as magnetic reconnection. This process is not only important for understanding the origin and evolution of the large-scale magnetic field, but is seen as a possibly efficient particle accelerator producing cosmic rays mainly through the first order Fermi process. In this work we study the properties of particle acceleration in reconnection zones and show that the velocity component parallel to the magnetic field of test particles inserted in nearly non-resistive magnetohydrodynamic (MHD) domains of reconnection without including kinetic effects, such as pressure anisotropy, the Hall term, or anomalous effects, increases exponentially. Also, the acceleration of the perpendicular component is always possible in such models. We have found that within contracting magnetic islands or current sheets the particles accelerate predominantly through the first order Fermi process, as previously described, while outside the current sheets and islands the particles experience mostly drift acceleration due to magnetic fields gradients. Considering two dimensional MHD models without a guide field, we find that the parallel acceleration stops at some level. This saturation effect is however removed in the presence of an out-of-plane guide field or in three dimensional models. Therefore, we stress the importance of the guide field and fully three dimensional studies for a complete understanding of the process of particle acceleration in astrophysical reconnection environments.

*Subject headings:* acceleration of particles — magnetic reconnection — magnetohydrodynamics — methods: numerical

## 1. INTRODUCTION

Acceleration of energetic particles is important for a wide range of astrophysical environments, from stellar magnetospheres, accretion disk/jet systems, supernova remnants and gamma ray bursts to clusters of galaxies. Several mechanisms for particle acceleration have been discussed in the literature which include varying magnetic fields in compact sources, stochastic second order Fermi process in turbulent interstellar and intracluster media, and the first order Fermi process behind shocks. An alternative, less explored mechanism so far, involves particle acceleration in magnetic reconnection sites, and this will be the focus of the present work which is a first of a series of papers on this subject. For a comprehensive recent review on particle acceleration mechanisms the reader is referred to Melrose (2009).

Magnetic reconnection may occur when two magnetic fluxes of opposite polarity encounter each other. In the presence of finite magnetic resistivity, the converging magnetic lines annihilate at the discontinuity surface and a current sheet forms there. It is common knowledge that magnetic fields stay frozen in highly conductive fluids. Estimates show that Ohmic diffusion for astrophysical scales is absolutely negligible, contributing to the strongly entrenched view that interacting magnetic fields of opposite polarity change their topology at low speeds. This is determined by the magnetic reconnection speed, and the famous example of two oppositely directed magnetic fluxes in Ohmic contact undergoing slow Sweet-Parker (Sweet 1958; Parker 1957) process of magnetic flux annihilation is frequently invoked. In a more generic context, the magnetic reconnection rate is the speed at which two

magnetic flux tubes, which are pushed against each other, can pass through altering the initial field topology. This is a situation that can be frequently encountered in astrophysical fluids with complex motions.

In the Sweet-Parker model, it has been shown that particles can accelerate due to the induced electric field in the reconnection zone (Litvinenko 2003). This *one-shot* acceleration process, however, is constrained by the narrow thickness of the acceleration zone which has to be larger than the particle Larmor radius and by the strength of the magnetic field. Therefore, the efficiency of this process is rather limited. Besides, it also does not predict a power-law spectrum, as generally observed for cosmic rays.

Observations have always been suggestive that magnetic reconnection can happen at a high speed in some circumstances, in spite of the theoretical difficulties in explaining it. For instance, the phenomenon of solar flares suggests that magnetic reconnection should be first slow in order to ensure the accumulation of magnetic flux and then suddenly become fast in order to explain the observed fast release of energy. A model that can naturally explain this and other observational manifestations of magnetic reconnection was proposed by Lazarian & Vishniac (1999). The model appeals to the ubiquitous astrophysical turbulence as a universal trigger and controller of fast reconnection. The predictions of the model have been successfully tested in numerical simulations by Kowal et al. (2009) which confirmed that this speed is of the order of the Alfvén speed in the presence of weakly stochastic magnetic field fluctuations.

An important consequence of fast reconnection of turbu-

lent magnetic fields<sup>1</sup> is the formation of a thick volume filled with reconnected small magnetic flux loops. Now, if such turbulent flow is immersed in a current sheet formed by two large scale converging magnetic flux tubes (such as, e.g., in the Sweet-Parker configuration), then the three-dimensional magnetic fluctuations or loops will contract and scatter test particles, presenting favorable conditions for energetic particle acceleration in a first order Fermi process. In other words, the particle may bounce back and forth between these converging magnetic mirrors formed by oppositely directed magnetic fluxes moving towards each other with the velocity corresponding to the reconnection speed. This has been first described in de Gouveia Dal Pino & Lazarian (2005) (see also Lazarian 2005) for the situation when there is no back reaction of the accelerated particles on the reconnected magnetic flux<sup>2</sup>. Later, Drake et al. (2006) appealed to a similar process, but within a collisionless reconnection scenario. In their model, the contraction of two-dimensional loops is controlled by the firehose instability that arises in the particle-in-cell (PIC) simulations containing both electrons and ions (Drake et al. 2010). In the present work, we show that this type of acceleration can be present in a pure magnetohydrodynamical scenario as well, where the pressure is fully isotropic and the contraction of islands is determined by their interactions.

Magnetic reconnection is ubiquitous in astrophysical circumstances and therefore it is expected to induce acceleration of particles in a wide range of astrophysical environments including galactic and extragalactic ones. For instance, the process has been already discussed for the production of ultra-high energy cosmic rays (de Gouveia Dal Pino & Lazarian 2000, 2001), acceleration of particles in gamma ray bursts (Lazarian et al. 2003; Zhang & Yan 2011), microquasars (de Gouveia Dal Pino & Lazarian 2005) and astrophysical jet-accretion disks in general (de Gouveia Dal Pino et al. 2010a,b). In particular, in the case of relativistic jets, a diagram of the magnetic energy rate released by violent reconnection as a function of the black hole (BH) mass spanning  $10^9$  orders of magnitude was derived and demonstrates that the magnetic reconnection power is more than sufficient to explain the observed radio outbursts, from microquasars to low luminous active galactic nuclei (AGN) (de Gouveia Dal Pino et al. 2010a).

More recently, the acceleration in reconnection regions has obtained observational support. It was suggested in Lazarian & Opher (2009) that anomalous cosmic rays measured by Voyagers are, in fact, accelerated in the reconnection regions of the magnetopause (see also Drake et al. 2010). Such a model explains why Voyagers did not see any signatures of acceleration passing the Solar system termination shock. In a separate development, Lazarian & Desiati (2010) have appealed to the energetic particle acceleration in the wake produced as the Solar system moves through interstellar gas to explain the excess of cosmic rays of the range of both sub-TeV and multi-TeV energies in the direction of the

magnetotail. Note, that due to the 11-year solar magnetic cycle the accumulation of magnetic reversals in the wake is unavoidable.

The implications of the acceleration process in reconnection sites are expected to be even much wider. Numerical two-dimensional (2D) simulations recently presented in Drake et al. (2010) confirmed the high efficiency of particle acceleration in regions of magnetic reconnection. However, we will show here that the process of acceleration happens rather differently in two and three dimensional (3D) situations. The 3D geometry shows a wider variety of acceleration regimes and this calls for much more detailed studies of the acceleration.

In Section 2 we describe the methodology of the particle acceleration studies presented here. In Section 3 we show the results obtained from these studies, in Sections 4 and 5 we discuss the results and draw the main conclusions of this work.

## 2. METHODOLOGY

In order to study particle acceleration in magnetic reconnection sites, we performed numerical simulations solving the isothermal magnetohydrodynamic (MHD) equations in two and three dimensions (2D and 3D, respectively). To compare our MHD results with those obtained with the Particle in Cell (PIC) code in Drake et al. (2010) we intentionally, in our 2D simulations, have reproduced their set up of eight Harris current sheets in a periodic box. The initial density profile is chosen in such a way that the total (gas plus magnetic) pressure is uniform. Initially, we imposed random weak velocity fluctuations to this environment in order to enable spontaneous reconnection events and the development of magnetic islands. We evolved the system in 2D (both without and with a guide field along the third dimension defined by  $Z$  direction) and in 3D domains. After the development of the magnetic loops (which in a 2D geometry form islands) in an underlying plasma configuration with defined density, velocity and magnetic field profiles, we injected test particles at a given snapshot and integrated their trajectories solving the equation of motion for each charged particle

$$\frac{d}{dt}(\gamma m \mathbf{u}) = q(\mathbf{E} + \mathbf{u} \times \mathbf{B}), \quad (1)$$

where  $m$ ,  $q$  and  $\mathbf{u}$  are the particle mass, electric charge and velocity, respectively,  $\mathbf{E}$  and  $\mathbf{B}$  are the electric and magnetic fields, respectively,  $\gamma \equiv (1 - u^2/c^2)^{-1/2}$  is the Lorentz factor, and  $c$  is the speed of light. In the studies below we assume that the charged particles are protons.

In the MHD simulations the electric field  $\mathbf{E}$  is generated either by the magnetized plasma or by resistive effects and can be obtained directly from the Ohm's law equation, i.e.,

$$\mathbf{E} = -\mathbf{v} \times \mathbf{B} + \eta \mathbf{j}, \quad (2)$$

where  $\mathbf{v}$  is the plasma velocity,  $\mathbf{j} \equiv \nabla \times \mathbf{B}$  is the current density, and  $\eta$  is the Ohmic resistivity coefficient.

In our studies we are not interested in the acceleration by the electric field resulting from resistivity effects, therefore we have neglected the last term in Equation (2) in the trajectory integration. The charged particles then feel an electric field  $\mathbf{v} \times \mathbf{B}$  besides the magnetic field. Substituting the Ohm's law, the equation of motion can be rewritten as

$$\frac{d}{dt}(\gamma m \mathbf{u}) = q[(\mathbf{u} - \mathbf{v}) \times \mathbf{B}]. \quad (3)$$

<sup>1</sup> This model of fast reconnection does not impose limits on the amplitude of magnetic perturbations. They can be small and the magnetic flux tubes require just to have a weak turbulent noise in order to produce fast magnetic reconnection, i.e., the reconnection which does not depend on Ohmic resistivity.

<sup>2</sup> This mechanism is in contrast to the second order Fermi acceleration which is frequently discussed in terms of the particle acceleration by turbulence generated by reconnection (La Rosa et al. 2006), (see also Kowal et al. 2011, in prep.).

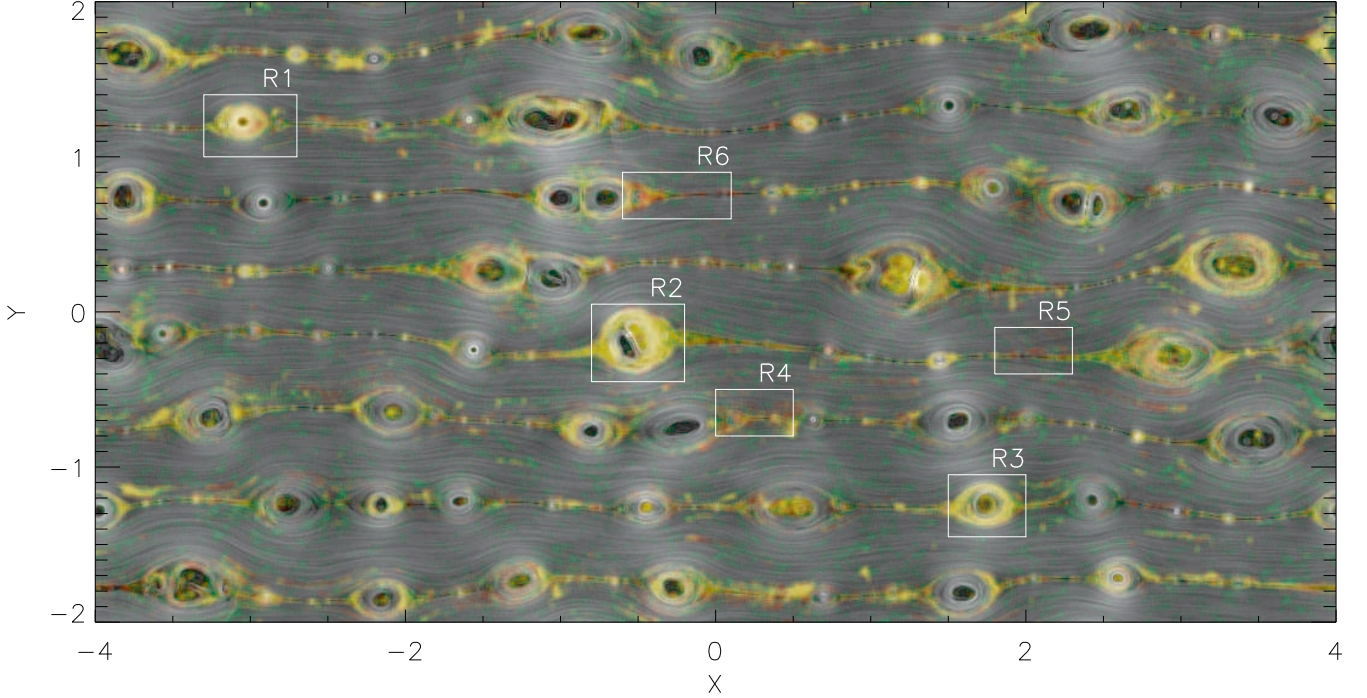


**Figure 1.** Topology of the magnetic field represented as the gray texture with semi-transparent color maps representing locations where the parallel and perpendicular particle velocity components are accelerated for a 2D model with  $B_z = 0.0$  at time 6.0 in the code units. The red and green colors correspond to regions where either parallel or perpendicular acceleration occurs, respectively, while the yellow color shows locations where both types of acceleration occur. The parallel component increases in the contracting islands and in the current sheets as well, while the perpendicular component increases mostly in the regions between current sheets. White boxes show regions that are more carefully analyzed in this paper. The simulation was performed with the resolution 8192x4096. We injected 10,000 test particles in this snapshot with the initial thermal distribution with a temperature corresponding to the sound speed of the MHD model.

The particle equation of motion (Eq. 3) was integrated using the 6<sup>th</sup> order implicit Runge-Kutta-Gauss (RKG) method (see Sanz-Serna & Calvo 1994, e.g.) with a fixed time step  $dt = 10^{-7}$ . The RKG methods are known to conserve the particle energy and momentum in very long integrations (Sanz-Serna & Calvo 1994) in contrast to the standard 4<sup>th</sup> order Runge-Kutta method with the adaptive time step based on the 5<sup>th</sup> order error estimator (see Press et al. 1992, e.g.), which is very commonly used.

The interpolation of the local values of the plasma velocity  $\mathbf{v}$  and magnetic field  $\mathbf{B}$  at each step of the integration has been done using cubic interpolation (Lekien & Marsden 2005) with our own discontinuity detector based on a total variation diminishing (TVD) limiter. We performed also the integration using linear interpolation which gave us essentially the same statistical results, but with much faster integration times.

In the current study we do not include particle energy losses, therefore test particles can gain or lose energy only through the interactions with the moving magnetized plasma and its fluctuations. The inclusion of radiative and non-radiative losses and also the back reaction of the particles on the plasma is planned for future studies.

For simplicity, we assume the speed of light to be 20 times the Alfvén speed  $V_A$ , which defines our plasma in a non-relativistic regime. The mean density is assumed to be 1 atomic mass unit per cubic centimeter which is compatible with the diffuse interstellar medium (ISM) density. The results are presented in units normalized by the assumed light speed and time unit (which is 1 hour in our simulations).

### 3. RESULTS

#### 3.1. Parallel and Perpendicular Acceleration in 2D Models

Figure 1 presents an evolved 2D configuration of the magnetic field structure with magnetic islands. We clearly see the merging of islands in some locations and the resulting deformations and/or contractions which provide appropriate conditions for particle acceleration in a similar way to the results obtained with the PIC code in (Drake et al. 2010, and references therein). In general, we distinguish two kinds of accelerating zones where one or both velocity components (parallel and perpendicular to the magnetic field) can increase.

In Figure 1, in order to demonstrate the zones which are favorable for a particular type of acceleration, we superimposed on top of the gray texture which represents the magnetic topology, a semitransparent color map showing the locations where acceleration increases the parallel (red) or the perpendicular (green) velocity component. In yellow areas, both types of acceleration can occur depending on the speed and direction of the test particle with respect to the orientation of the magnetic field lines.

We see that the increase of the parallel velocity component is mostly observed within deformed islands and in current sheets (see the red and yellow zones in Figure 1), while the increase of the perpendicular component is observed mostly near and within the islands and between current sheets (see the green and yellow zones in Figure 1). This complex behavior is related to the degree of island deformation and the particle direction and speed. If the island contracts, the particle can increase its parallel component, however, when the island increases its deformation the preferable acceleration usually takes place in the perpendicular direction. Interestingly, we can find islands in which the acceleration does not happen at

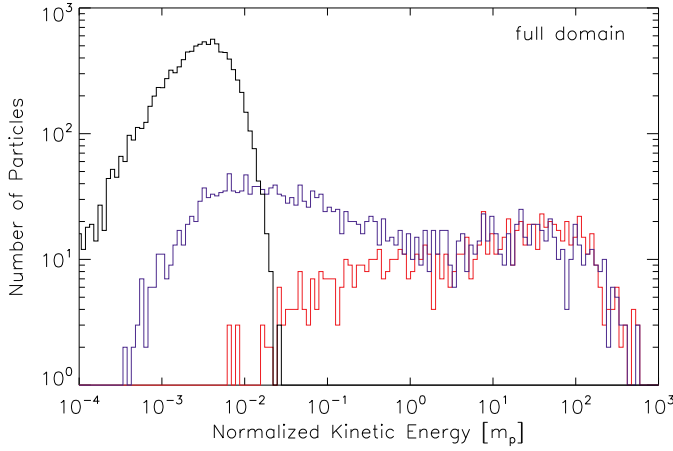


**Figure 2.** Particle energy distributions in the full domain of Figure 1. Blue and red histograms show the number of particles accelerating their perpendicular and parallel velocity components, respectively, at one hour after the particles injection in the system. The black line exhibits the initial thermal distribution of the injected particles.

all (see, e.g., the islands above and below the region R3 in Figure 1). This is due to the fact that these islands are not undergoing contraction or deformation processes.

### 3.2. Distribution of the Accelerated Particles

In Figure 2 we present the energy distribution of all particles of the domain of Figure 1 at a time corresponding to 1 hour after the injection, when the particles are still accelerating. The red and blue lines show the number of particles which increase their parallel and perpendicular velocity components, respectively, as a function of the kinetic energy. In addition, we show the initial thermal distribution of particles (black line).

In the particle energy distribution corresponding to the perpendicular acceleration component (blue), we distinguish two modes, one in the low energy range which is related to the initially injected thermal distribution with an extended non-thermal tail, and the other corresponding to the high energy range. For the particle energy distribution corresponding to the parallel acceleration component, we see only one distribution mode with a maximum at high energies. In the low energy range with energies smaller than the particle rest mass energy (around  $10^{-2}$ ), there is a clear dominance of the perpendicular acceleration. This creates an anisotropy between the two velocity distributions with respect to the magnetic field. However, once the particles become relativistic and their kinetic energies become comparable to or larger than the particle rest mass energy, the anisotropy disappears and the acceleration in both directions is equally efficient.

Figure 3 presents the energy distributions of accelerated particles in the selected regions R1 to R6, as shown in Figure 1. Regions R1 to R3 correspond to islands where both parallel and perpendicular accelerations are observed, while regions R4 to R6 correspond to current sheets.

The energy distributions for regions R1 to R3 are shown in the top panels of Figure 3. We notice a dominance of the perpendicular acceleration in the low energy range, similarly as seen in Figure 2. As we move to higher energies we see a trend to form a saturated tail. The efficiency of the acceleration of the parallel component increases with the particle energy and at the highest energies the number of particles accelerating in the parallel and perpendicular directions is com-

parable.

In the bottom panels of Figure 3 we present the particle energy distributions for regions within current sheets which are labeled as R4, R5, and R6 in Figure 1. In these cases, we also observe an anisotropy between the perpendicular and parallel components in the low energy range with a dominance of the perpendicular acceleration. As in the case of the whole domain, this anisotropy decreases with increasing energy and, beyond values around the particle rest mass energy both component distributions become comparable. The high energy range tails of these distributions are steeper than those of the top diagrams of the figure which correspond to magnetic islands. This is especially well seen in the energy distribution of region R6. This indicates that the number of accumulated particles in the high energy range is smaller and therefore the acceleration, although still significant, is less efficient in current sheets than within the islands. This is apparently due to the fact that (at least in the 2D case) the islands are able to retain the particles trapped for longer times. What could be the dominant mechanism(s) for the acceleration in these zones?

The acceleration in the contracting/deforming islands is suggestive of first order Fermi processes with the particles bouncing back and forth between converging mirrors as described in de Gouveia Dal Pino & Lazarian (2005) and Drake et al. (2010), while within and between the current sheets the acceleration mechanism is not as clear. In the following sections, we will examine the acceleration mechanism in these different sites in more detail.

### 3.3. Acceleration in Contracting Islands

In Figure 4, we show an example of a test proton which is trapped in a contracting island and accelerates increasing its parallel component. The left panel of the figure shows the topology of the magnetic field in a region with a contracting island (R1 in Fig. 1) with the trajectory of the proton superimposed. As long as the proton remains trapped in the island it orbits around the island center. In the middle panel we plot the evolution of the parallel and perpendicular velocity components (red and green lines, respectively), and the kinetic energy evolution (blue line) of the test particle. In the right panel, we plot the change of the kinetic energy with the particle X coordinate. While trapped in the island, the particle orbits around the center and increases its energy after each cycle. Its parallel speed increases while the gyro rotation slows down. This results in an exponential growth of the kinetic energy of the particle (see middle panel). If we take a closer look in the change of the kinetic energy with the position we see that the increase of energy happens only when the particle moves across the right part of the island. The left panel showing the magnetic field topology indicates that the field lines in this part are contracting due to the interaction with a small island which is merging with the central one. At the same time, the particle gains more energy after each pass in this zone.

We clearly see how easily the results of Drake et al. (2010) can be reproduced using the MHD approximation, confirming that the process of acceleration in the islands is not restricted to the collisionless physics described by PIC codes. MHD codes present an easier way to study the physics of particle acceleration numerically.

### 3.4. Acceleration Near and Within Current Sheets

We know from shock acceleration theory that particles are injected upstream and allowed to convect into the shock,



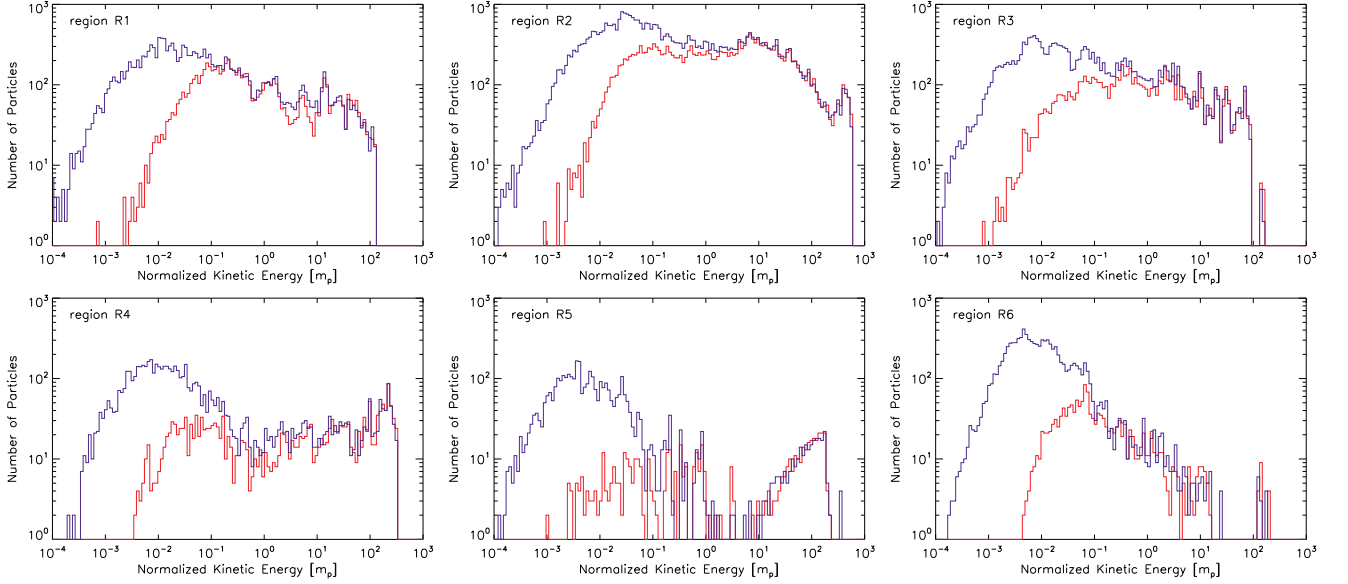


**Figure 3.** Particle energy distributions in the selected regions of Figure 1. Blue and red histograms correspond to the number of particles which accelerated their perpendicular and parallel velocity components, respectively. These histograms are created for all accelerating particles passing through this region from the injection moment until 1 hour.

while diffusing in space so as to effect multiple shock crossings, and thereby gain energy through the first order Fermi process. Now, besides this mechanism, they may also experience shock drift acceleration, which is attributed to the grad-B drift when the particle encounters an abrupt change in magnetic fields. The origin of this effect is due to the net work done on a charge by the Lorentz force (Eq. 2) in a zone of non-uniform large scale magnetic field. The principal equation governing this is the scalar product of the particle velocity (or momentum) and the acceleration by the convective electric field,  $-q\mathbf{v} \times \mathbf{B}$ . In uniform magnetic fields, the energy gain and loss acquired during a gyroperiod exactly cancel, so in result no net work is done,  $\Delta W = 0$ .

In contrast, when the gyromotion of a charged particle straddles a discontinuity, the sharp field gradient induces an asymmetry in the time spent by the charge in either side of the discontinuity, so that energy gain and loss do not compensate each other. The compressive nature of the field discontinuity biases the net work done to positive increments in shock encounters between upstream excursions, and it can be shown that  $\Delta W = qE_x dx$ , where the  $\mathbf{v} \times \mathbf{B}$  drifts lie in the x-direction, in other words, this energy gain scales linearly with displacement along the drift coordinate x (i.e., along the discontinuity). Thus the energy gained by a particle depends on how far it drifts along the front (see, e.g., Baring & Summerlin 2009; Lugones 2011, and references therein).

Similarly, in the current sheet zones (regions R4 to R6) we may be identifying two distinct mechanisms of acceleration, either first order Fermi acceleration in contracting/merging islands which are just forming there (or even the simple particle scattering between the converging flows entering both sides of the current sheet, as described in de Gouveia Dal Pino & Lazarian 2005), or a drift acceleration, as described above. The islands in current sheets are smaller than those of regions R1, R2 and R3, what results in smaller acceleration rates as we see in the lower panels of Figure 3. In the zones above and below the current sheets it is possible that we see predominantly a drift acceleration driven by non-uniformities of the magnetic field. Generally,

this effect is less efficient than the first order Fermi process in merging/contracting islands and results in smaller acceleration rates.

In order to better understand these distinct acceleration mechanisms, we have also explored the details of the acceleration of a test particle near and within a single (Sweet-Parker shaped) current sheet. Figure 5 shows the trajectory and energy evolution of this test particle. We see that before the particle reaches the current sheet discontinuity it is drifted by the plasma inflow and the increasing gradient of B as it approaches the current sheet. When it enters the discontinuity (the white part of the trajectory in the left panel), it bounces back and forth several times and gains energy (which increases exponentially as shown in the middle panel of Figure 5) due to head-on collisions with the converging flow, on both sides of the magnetic discontinuity (i.e., in a first order Fermi process, as described in de Gouveia Dal Pino & Lazarian 2005). At the same time it drifts along the magnetic lines which eventually allow it to escape from the acceleration region. Therefore, we see two mechanisms: a drift acceleration (dominating outside of the current sheet) and first order Fermi acceleration inside the current sheet. These processes naturally depend on the initial particle gyroradius, since it determines the amount of time the particle remains in the acceleration zone before escaping.

Finally, we may also argue that turbulence above and below the current sheets in Figure 1, far from the islands and diffusion regions, favor second order Fermi acceleration mechanisms with particles being scattered by approaching and receding magnetic irregularities. Nevertheless, the first order Fermi processes occurring within the islands and current sheets dominate the overall particle acceleration in the system.

### 3.5. The Role of a Guide Field: 2D vs. 3D simulations

The results presented in the previous sections were obtained for 2D models without a guide field. This means that in this case the magnetic lines creating the islands are closed and a charged particle can be trapped indefinitely in such an island. The presence of a guide field normal to the plane of Figure 1

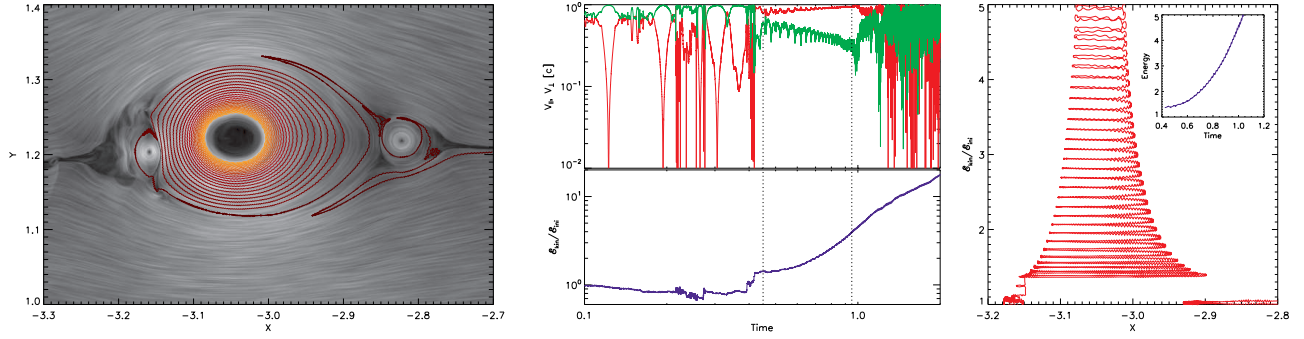


**Figure 4.** The case of a contracting island where the particles accelerate efficiently (region R1 of Fig. 1). In the left panel we show the trajectory of a test proton trapped in a contracting island. We see two small magnetic islands on both sides of the central elongated island which are merging with it. This process results in the contraction of the central island. In the middle panel we show the evolution of the parallel and perpendicular speeds of the test proton (red and green lines, respectively) and the evolution of the particle energy (blue line). In the right panel it is shown the change of the particle kinetic energy with the X coordinate. The proton orbiting around the center of the magnetic island increases its energy increment after each orbit.

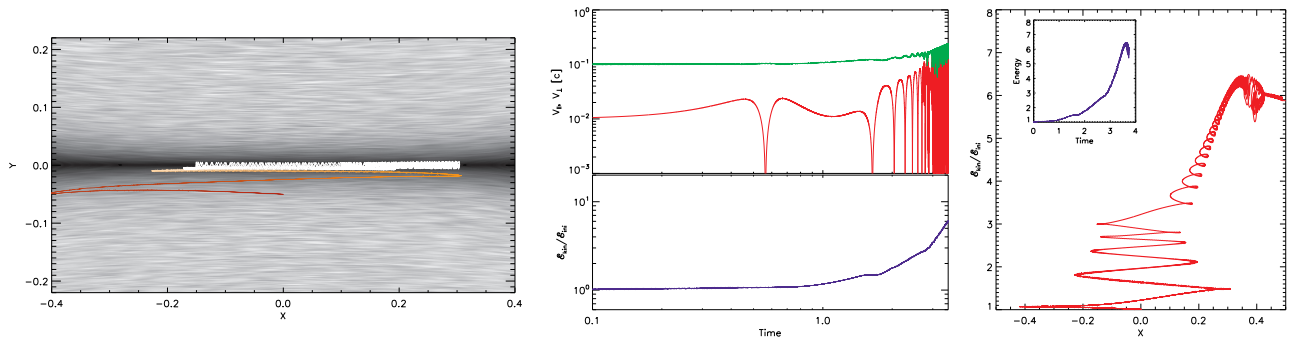


**Figure 5.** The case of acceleration near and within a single current sheet with a Sweet-Parker configuration where the particles accelerate efficiently (like region R6 of Fig. 1). The left panel shows the trajectory of a test proton approaching the diffusion region. The color of trajectory corresponds to the particle energy (which increases from red to yellow and then finally to white when the particle reaches the current sheet). The middle panel shows the evolution of the parallel and perpendicular speeds of the test proton (red and green lines, respectively) and the evolution of the particle energy (blue line). The right panel shows the change of the particle kinetic energy with the X coordinate. Outside the current sheet the proton drifts under the effect of the magnetic field gradients and then when it arrives in the current sheet it bounces back and forth between the converging magnetic fluxes of opposite polarity while drifting along the magnetic field.

opens the magnetic loops and allows the charged particles to travel freely in the out-of-plane direction. Moreover, the islands evolve much slower in the presence of a strong guide field.

In Figure 6, we present the time evolution of the kinetic energy of the particles which have their parallel and perpendicular (red and blue points, respectively) velocity components accelerated for three models of reconnection. The upper panel shows the energy evolution for a 2D model without the guide field (as in the models studied in the previous sections). Initially, the particles pre-accelerate by increasing their perpendicular velocity component only. However, later there is an exponential growth of energy mostly due to the acceleration of the parallel component which stops after the energy reaches values of  $10^3$ – $10^4 m_p$  (where  $m_p$  is the proton rest mass energy). From that level on, particles accelerate their perpendicular component only with smaller linear rate in a log-log diagram. The middle panel shows the kinetic energy evolution in a 2D model with a weak guide field  $B_z=0.1$  normal to the plane of Figure 1. In this case, there is also an initial slow acceleration of the perpendicular component followed by the exponential acceleration of the parallel velocity component. However, due to the presence of a weak guide field, the parallel component accelerates further to higher energies at a similar rate as the perpendicular one. This implies that the presence of a guide field removes the restriction seen in the 2D model without a guide field and allows the particles

to increase their parallel velocity components as they travel along the guide field, in open loops rather than in confined 2D islands. This result is reassured by the 3D model in the bottom panel of Figure 6, where no guide field is necessary as the MHD domain in fully three-dimensional. In this case, we clearly see a continuous increase of both components, which suggests that the particle acceleration behavior changes significantly when 3D effects are considered, where open loops replace the closed 2D reconnecting islands.

Considering the parametrization we have chosen for our models, the gyroradius of a proton becomes comparable to the size of the box when its Lorentz factor reaches a value of a few times  $10^4$ . The largest islands in the system can have sizes of a few tenths of the size of the box. These rough estimates help us to understand the energy evolution in Figure 6 and the transition from an exponential to a much slower (linear) growth rate in the energy around 10 hours. We note that in the diagrams of this figure, the energy is normalized by the rest mass value, so that in fact, it is the Lorentz factor that is plotted. In the case with absence of a guide field (top panel of Fig. 6), the exponential parallel acceleration stops right before the energy value  $10^4$  is reached. After this, the rate of acceleration significantly decreases. This occurs because the Larmor radius of the particles has become larger than the sizes of biggest islands. Therefore, from this level on the particles cannot be confined anymore within the islands and the first order Fermi acceleration ceases. After that, there is a

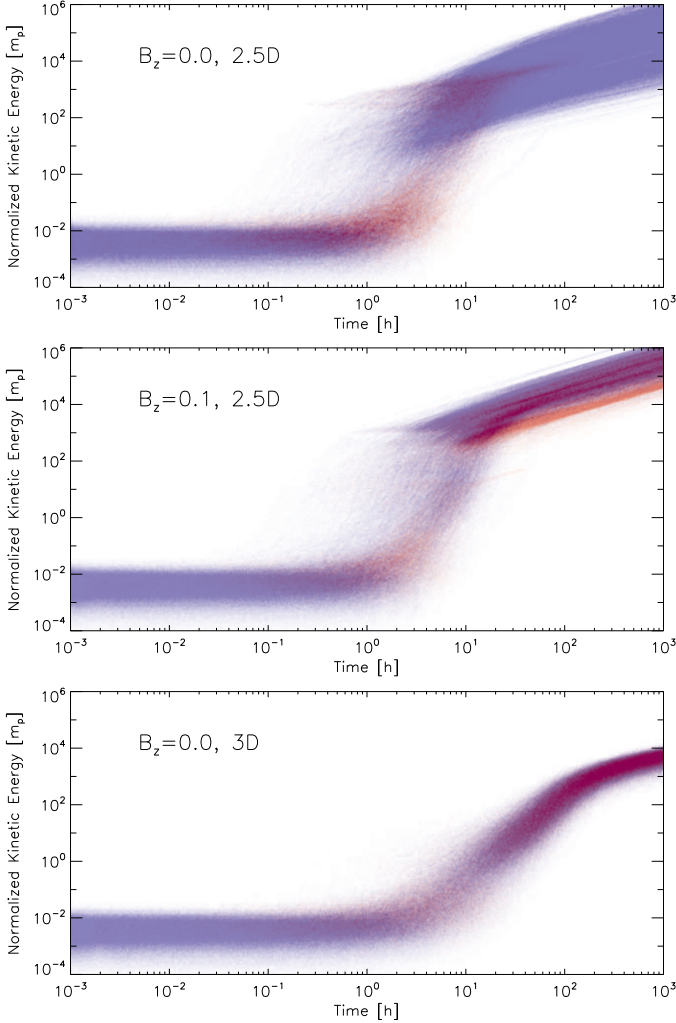


**Figure 6.** Kinetic energy evolution of a group of  $10^4$  protons in 2D models of reconnection with a guide field strength  $B_z=0.0$  and  $0.1$  (top and middle panels, respectively). In the bottom panel a fully 3D model with initial  $B_z=0.0$  is presented. The colors show how the parallel (red) and perpendicular (blue) components of the particle velocities increase with time. The energy is normalized by the rest proton mass energy. The background magnetized flow with multiple current sheet layers is at time 4.0 in Alfvén time units in all models.

much slower drift acceleration (of the perpendicular component only) caused by the gradients of the large scale magnetic fields. If a guide field is inserted in such a system, the picture is very similar, except for one detail. Now, since the particles are able to travel along the guide field, their parallel velocity component also continues to increase after the  $10^4$  threshold (see the middle panel of Fig. 6). Of course, in the 3D model, the particles follow the same trend (bottom panel of Fig. 6).

Figure 7 exhibits the dependence of the acceleration rate on the out-of-plane guide field strength. It shows the particle kinetic energy distribution for three models of reconnection with different strengths of the guide field ( $B_z=0.0$ ,  $0.5$ , and  $1.0$  for the top, middle, and bottom panels, respectively) 1 hour after the injection. The initial injected thermal distribution is represented by the blue line. The particles trajectory integration was performed at the same MHD snapshot, at time 4.0 (in units of Alfvén time), for all particles in these models. We note that at the final state the particle distributions have developed high energy tails which depart from the initial ther-

mal distribution. However, both the number of accelerated particles to higher energies and the maximum energy at the final time interval strongly depends on the strength of the guide field.

#### 4. DISCUSSION

In this paper we have investigated the process of particle acceleration in reconnection zones considering test particles inserted in an isothermal magnetohydrodynamic domain containing a series of reconnection layers, without including kinetic effects. There were a few goals that motivated our approach. The first goal was to study if the contraction of magnetic islands, which develop in 2D reconnection layers with finite resistivity, can also occur when the gas pressure is isotropic, as is the case in the MHD regime. In earlier studies, Drake and collaborators (Drake et al. 2010) invoked kinetic effects such as the firehose and mirror instabilities to control the development and contraction of the islands in current sheets. In the present work, after obtaining the formation of contracting/deformed islands in current sheets in a nearly incompressible MHD domain, the second goal was to investigate the acceleration of test particles particularly in the direction parallel to the large scale magnetic fields during island contractions. We were able to identify several regions where such acceleration occurs both in a 2D environment with and without a guide field and in a 3D environment. Also, we were able to identify the nature of the acceleration mechanisms in the different acceleration regions, not only within the contracting islands, but also near and inside the current sheets. We found that first order Fermi processes occur in the islands and also within the current sheets, while drift acceleration due to magnetic field gradients seems to be dominating outside the current sheets.

Our results for particle acceleration in 2D MHD models were quite similar to those obtained by Drake et al. (2010), i.e., during an island contraction, in our case resulting from the merge with other islands, a particle trapped in it can accelerate and increase its energy exponentially and its parallel velocity component grows while the perpendicular one undergoes a net decrease. During this process the energy gain is proportional to the particle energy. These are all necessary conditions in a Fermi like process and a close examination of the motion of a test particle in a contracting island shows clear evidence of the first order Fermi acceleration process.

Similarly, exponential acceleration of the parallel velocity component was also detected in regions within the current sheets. A detailed examination of a test particle trajectory within and near a current sheet revealed that outside the discontinuity the particle experiences drift acceleration due to magnetic field gradients and within the current sheet it goes back and forth between the converging flows on both sides of the discontinuity also gaining energy exponentially, just as described in de Gouveia Dal Pino & Lazarian (2005), while drifting along the magnetic field direction.

Drake et al. (2010) have claimed that particle acceleration in an X-point reconnection in a 3D environment, even in the presence of a guide field, should behave like in 2D systems. However, we have shown that in the presence of an out-of-plane guide field, this picture changes completely (see also Drake et al. 2010). While in 2D MHD models without a guide field the parallel acceleration stops after reaching a certain energy threshold, in 2D MHD models with a guide field this constraint is removed, and particles can continue increasing their parallel speed as they travel along the guide field. Fur-

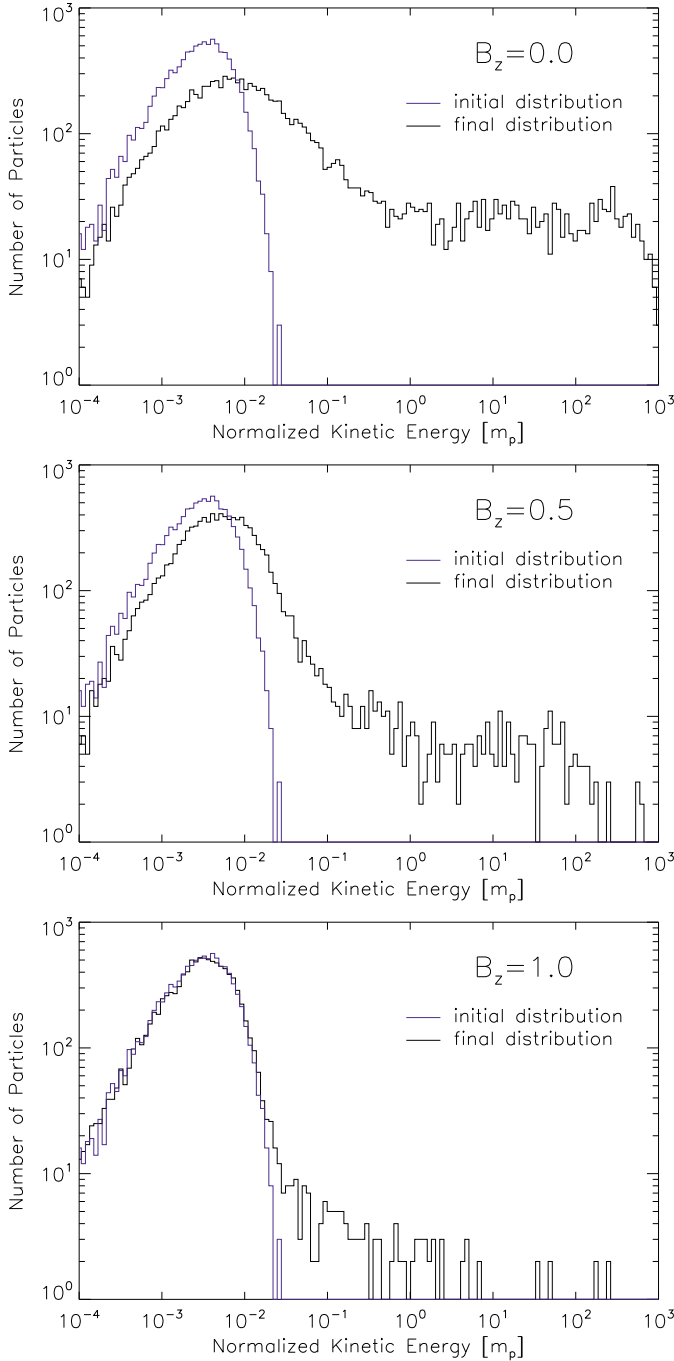


**Figure 7.** Kinetic energy distribution of the particles for three 2D models with different strengths of the out-of-plane guide field  $B_z = 0.0, 0.5$ , and  $1.0$  (top, middle and bottom panels, respectively.) at a time corresponding to 1 hour after the injection. The initial particle thermal distribution is given by the blue line.

thermore, in fully 3D MHD models with no guide field the acceleration of the particles exhibits the same trend as in 2D models with a guide field, i.e., there is no constraint on the acceleration of the parallel speed. This result is very important as it implies that the overall picture of particle acceleration in 3D reconnection can be very distinct from that in 2D reconnection. Also, it can offer some important clues for particle acceleration in more complex domains, such as in the presence of 3D turbulence where stochastic reconnection is

involved (see Kowal et al. 2011, in prep.).

Another important result of the present work was to demonstrate that the investigated acceleration mechanisms in reconnection sites (both drift and Fermi processes) can be present in any environment whose evolution can be approximated by a nearly ideal MHD description as employed here, therefore, without the necessity of invoking kinetic instabilities or anomalous resistivity effects to control the pressure anisotropy or the reconnection rate. The nearly non-resistive MHD approach with test particle injection offers a possibility of exploring more realistic systems. Even though PIC codes in general allow the study of plasma processes in greater detail, they present some disadvantages with regard to an MHD description, such as the necessity of a much higher complexity in the 3D modeling, for instance, of turbulence.

A final remark is in order. Onofri et al. (2006) investigated particle acceleration in reconnection zones and concluded that MHD should not be a good approximation to describe the whole process of acceleration. However, their 3D numerical simulations were performed in a fully resistive MHD regime. Therefore, they obtained very efficient particle acceleration due to the high electric field induced by resistivity and an absorption of most of the available magnetic energy by the electrons in a very small fraction of the characteristic time of the MHD simulation. This led them to conclude that resistive MHD codes are unable to represent the full extent of particle acceleration in 3D reconnection. In the present work, we have investigated particle acceleration in a nearly ideal MHD regime where only numerical resistivity is present. In this case, the contribution of a resistivity induced electric field is negligible when compared to the advection component, namely, the electric field resulting from the plasma motion in the magnetized medium,  $\mathbf{E} = -q\mathbf{v} \times \mathbf{B}$ . Moreover, since there is no important dissipation effects, our model is scale independent and allows for dimensionless units, so that it is straightforward to rescale the configuration to reproduce different astrophysical environments. The main drawback of the numerical resistivity is the creation of a “hole” in the center of the magnetic islands, since the numerical modeling cannot handle properly the strongly curved magnetic lines over a few cells. As a consequence, numerical dissipation removes part of the magnetic flux in this region.

The importance of the present study of acceleration in the MHD regime is motivated by the fact that magnetic reconnection in 3D becomes fast according to the model in Lazarian & Vishniac (1999) (see also Lazarian et al. 2004). This model has been successfully tested via numerical simulations in Kowal et al. (2009) which confirmed that thick reconnection layers form, where magnetic energy is transferred into energy of contracting loops<sup>3</sup>. In the present paper, we have confirmed that these loops (or magnetic irregularities) can act as the places of efficient particle acceleration providing the support for the mechanism first discussed in de Gouveia Dal Pino & Lazarian (2005). At the same time, we see that the process of acceleration does not amount to only the process of first order Fermi acceleration outlined in the aforementioned paper. Our simulations show a complex interplay of different acceleration processes, which motivates for further studies of the acceleration in the presence of realistic turbulent reconnection (see Kowal et al. 2009).

The present study has clearly an exploratory character. It

<sup>3</sup> These thick layers were also confirmed by Ciaravella & Raymond (2008).



testifies that the acceleration in reconnection regions may be more complex than it may be inferred from earlier simplified 2D studies. Further study of the acceleration in the MHD regime is absolutely essential, as ubiquitous astrophysical turbulence is expected to induce magnetic reconnection all over astrophysical volumes and should be explored in more detail. In this situation the acceleration of particles by reconnection may play a vital role, the extend of importance of which can be evaluated from further research (Kowal et al. 2011).

### 5. SUMMARY

The results of the paper can be very briefly summarized as follows:

- Advances in the understanding of magnetic reconnection in the MHD regime, in particular, turbulent magnetic reconnection in Lazarian & Vishniac (1999) model motivate the studies of whether the reconnection in this regime can accelerate energetic particles.
- Contracting magnetic loops in magnetic reconnection in 2D, in the MHD regime, provides the acceleration which successfully reproduces the results obtained earlier with more complicated PIC codes, which proves that the acceleration in reconnection regions is a universal process which is not determined by the details of plasma physics.
- Acceleration of energetic particles in 2D and 3D shows substantial differences, which call for focusing on realistic 3D geometries of reconnection. Our study also shows that apart from the first order Fermi acceleration, additional acceleration processes interfere.

GK and EMGDP acknowledge the support by the FAPESP grants no. 2006/50654-3 and 2009/50053-8, and the CNPq grant no. 300083/94-7, and AL thanks the NSF grant AST 0808118, NASA grant NNX09AH78G and the support of the Center for Magnetic Self Organization. This research was also supported by the project TG-AST080005N through TeraGrid resources provided by Texas Advanced Computing Center (TACC:<http://www.tacc.utexas.edu>). Part of the computations presented here were performed on the GALERA su-

percomputer in the Academic Computer Centre in Gdańsk (TASK:<http://www.task.gda.pl/>).

### REFERENCES

- Baring, M. G. & Summerlin, E. J. 2009, in AIP Conf. Proc. Ser. 1183, Shock Waves in Space and Astrophysical environments: 18th Annual International Astrophysics Conference, ed. X. Ao & G. Z. R. Burrows (Melville, NY:AIP), 74
- Ciaravella, A., & Raymond, J. C. 2008, ApJ, 686, 1372
- de Gouveia Dal Pino, E. M. & Lazarian, A. 2000, ApJ, 536, L31
- de Gouveia Dal Pino, E. M. & Lazarian, A. 2001, ApJ, 560, 358
- de Gouveia Dal Pino, E. M. & Lazarian, A. 2005, A&A, 441, 845
- de Gouveia Dal Pino, E. M., Piovezan, P. P. & Kadowaki, L. H. S. 2010a, A&A, 518, A5
- de Gouveia Dal Pino, E. M., Kowal, G., Kadowaki, L. H. S., Piovezan, P., & Lazarian, A. 2010b, International Journal of Modern Physics D, 19, 729
- Drake, J. F., Swisdak, M., Schoeffler, K. M., Rogers, B. N., & Kobayashi, S. 2006, Geophys. Res. Lett., 33, 13105
- Drake, J. F., Opher, M., Swisdak, M., & Chamoun, J. N. 2010, ApJ, 709, 963
- Kowal, G., Lazarian, A., Vishniac, E. T., & Otmianowska-Mazur, K. 2009, ApJ, 700, 63
- Kowal, G., de Gouveia Dal Pino, E. M. & Lazarian, A. 2011, in prep.
- La Rosa, T. N., Shore, S. N., Joseph, T., Lazio, W., & Kassim, N. E. 2006, Journal of Physics Conference Series, 54, 10
- Lazarian, A. 2005, in AIP Conf. Proc. Ser. 784, Magnetic Fields in the Universe: From Laboratory and Stars to Primordial Structures, ed. E. M. de Gouveia dal Pino, G. Lugones, & A. Lazarian (Melville, NY:AIP), 42
- Lazarian, A. 2006, Astronomische Nachrichten, 327, 609
- Lazarian, A. & Vishniac, E. T. 1999, ApJ, 517, 700
- Lazarian, A., Petrosian, V., Yan, H. & Cho, J. 2003, Review at the NBSI workshop "Beaming and Jets in Gamma Ray Bursts", Copenhagen, August 12-30, 2002 (arXiv:astro-ph/0301181)
- Lazarian, A., Vishniac, E. T., & Cho, J. 2004, ApJ, 603, 180
- Lazarian, A. & Opher, M. 2009, ApJ, 703, 8
- Lazarian, A. & Desiati, P. 2010, ApJ, 722, 188
- Lekien, F., & Marsden, J. 2005, International Journal for Numerical Methods in Engineering, 63, 455
- Litvinenko, Y. E. 2003, Sol. Phys., 216, 189
- Lugones, G. 2011, Procs. of Science, in press
- Mackay, F., Marchand, R., & Kabin, K. 2006, J. Geophys. Res., 111, A106205
- Melrose, D. B. 2009, in press (arXiv:0902.1803)
- Onofri, M., Isliker, H., & Vlahos, L. 2006, Phys. Rev. Lett., 96, 151102
- Parker, E. N. 1957, J. Geophys. Res., 62, 509
- Press, W. H., Teukolsky, S. A., Vetterling, W. T., & Flannery, B. P. 1992, *Numerical recipes in C (2nd ed.): the art of scientific computing*, Cambridge University Press, New York, NY, USA
- Sanz-Serna, J. M. & Calvo, M. P. 1994, *Numerical Hamiltonian Problems*, Chapman & Hall, London, UK
- Sweet, P. A. 1958, in IAU Symp. 6, Electromagnetic Phenomena in Cosmical Physics, ed. B. Lehnert (Cambridge: Cambridge Univ. Press), 123
- Yugo, H. & Iyemori, T. 2001, J. Geophys. Res., 106, 26075
- Zhang, B. & Yan, H. 2011, ApJ, 726, 90